Escola de Primavera de Transição e Turbulência
Blumenau 2020

ABCM Associação Brasileira de Engenharia e Ciências Mecânicas

12th Spring School on Transition and Turbulence
September 21st-25th, 2020, Blumenau, SC, Brazil

# EPTT-2020-0128
# ON THE CALIBRATION OF THE KINETIC ENERGY-HELICITY TURBULENCE MODEL

**José Ricardo Figueiredo**
**Unicamp, FEM (retired)**
**jrfigue@fem.unicamp.br**

***Abstract.*** *A proposed turbulence model is based on the transport equations for the fluctuating kinetic energy and helicity, together with the statistical dynamic equation for the velocity-vorticity tensor, which is related to the divergence of the Reynolds stress. This work reports on initial steps towards constructing the computational tools for the calibration of such model. Actual calibration requires DNS or LES methods, which demands parallel processing in computational cluster, whilst the work here presented was performed in a personal computer, simulating turbulent fluctuations by a laminar oscillating flow. The incompressible isothermal Navier-Stokes solver uses the semi-staggered mesh, the UNIFAES scheme for the discretization of advective and viscous terms of momentum equation, the Poisson equation for pressure to enforce continuity, and forth order Runge-Kutta integration of the momentum equation. Correlations being recorded are the fluctuating parts of kinetic energy and helicity, all terms of the respective transport equations, and the terms of the statistical dynamic equation for the velocity–vorticity tensor. These are computed with both second and forth order central differencing, and Simpson´s integration rule for the statistical dynamic equations. Intensive checking is performed by comparing conceptually equivalent but numerically distinct expressions, such as advective and divergence forms of the advective terms, and others.*

***Keywords:*** *helicity, kinetic energy, velocity-vorticity tensor*

## 1. INTRODUCTION

The construction of a kinetic energy – helicity turbulence model was advocated in previous paper (Figueiredo, 2018a). Briefly, helicity is defined as the scalar product of velocity and vorticity. Analogous to energy, helicity presents a conservation principle in inviscid flows. It has been a fruitful concept in meteorology and magneto-hydrodynamics, and its presence has been observed in physics literature about turbulence. It can be positive or negative valued, being a measure of the asymmetry of the flow, feature essential to turbulence phenomena which is not captured by the strictly positive scalars kinetic energy and energy dissipation rate, specific dissipation or enstrophy, which are used in present RANS and LES models.

The transport equation for fluctuating helicity is dependent on the mean vorticity, but not on the mean shear, forming a consistent pair with the transport equation for fluctuating kinetic energy, which depends on mean shear but not on mean vorticity. Vortex stretching, which is fundamental for turbulence decay, involves variations in the velocity and vorticity fields, being necessarily influenced by the fluctuating velocity-vorticity correlation.

Helicity is the trace of the velocity-vorticity tensor, whose skew-symmetric part is associated to the divergence of the Reynolds stress, required for the mean momentum equation. The deviatoric components of the velocity-vorticity tensor are also related to the Magnus effect (Tennekes and Lumley, 1972). Both vortex stretching and Magnus effects are present in the quasi-coherent structure called “hairpin vortex” observed on wall bounded flows, which begins very near the solid surface and extends to the order of magnitude of the boundary layer (Pope, 2000, Davidson, 2004). The vortex rising is due to the Magnus effect. Left Fig.1 sketches typical mean velocity and mean vorticity profiles in a boundary layer; velocity increases upward whilst vorticity decreases. The small black circle represents a vortex tube in direction $x_3$ , corresponding to the strait first filament in the right side of Fig. 1. Suppose a small perturbation displaces part of the filament upwards, as indicated in the second filament. This part is placed in a region of smaller vorticity but higher velocity, so that the Magnus effect starts to act, causing further displacement. The higher the vortex goes the stronger the Magnus effect, which so appears as the cause of instability that creates the hairpin shape. Vortex stretching results from advection with distinct mean velocities.

The proposal of the kinetic energy – helicity turbulence model is complemented by the statistical dynamic equation method to pursue the algebraic relations of the model, particularly for the velocity-vorticity tensor; such method has been applied with success to the turbulent transport of kinetic energy in shear flows (Figueiredo, 2016, 2018a).

Calibration of the model must employ DNS or LES, requiring clusters for parallel computation. However, the work reported here refers to the initial steps of the construction of the algorithms for computing the numerous statistical

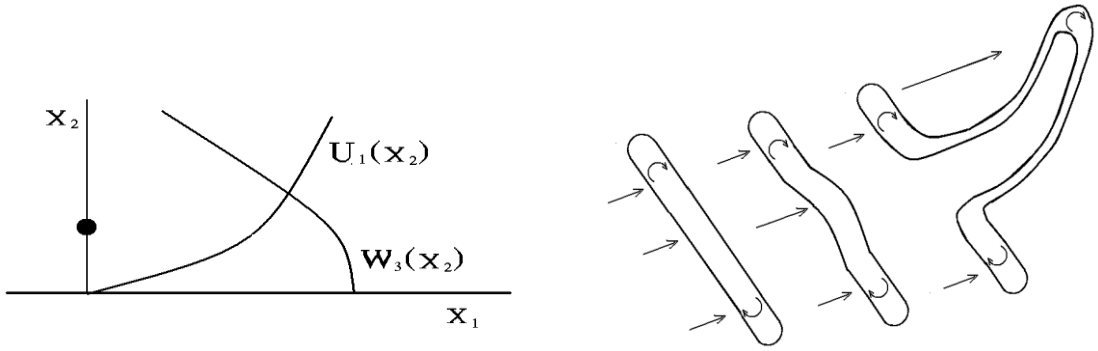


Fig. 1 – Left: sketch of boundary layer mean velocity and vorticity, marking a vortex tube. Right: development of a small perturbation of the vortex tube into the hairpin shape.

correlations, which is being performed with a personal computer. Within this limitation, turbulent situations cannot be effectively reproduced, and the testing of the statistics program is performed in oscillating laminar flows, where the initial difficulties can be appreciated, and the algebraic and programming correctness of the correlations can be verified. Of course, the mathematical operations of the Reynolds decomposition are valid for oscillating laminar flows. Although the resulting terms do not correspond quantitatively to turbulent flows, they will be referred according to the turbulent terminology.

## 2. NAVIER-STOKES SOLVER

For incompressible isothermal Newtonian flows the continuity and Navier-Stokes equations are expressed as:

$$\frac{\partial \mathcal{U}_j}{\partial x_j} = 0 \tag{1}$$

$$\frac{\partial \mathcal{U}_i}{\partial t} = -\frac{\partial (\mathcal{U}_i \mathcal{U}_j)}{\partial x_j} + \frac{1}{Re}\frac{\partial^2 \mathcal{U}_i}{\partial x_j \partial x_j} - \frac{\partial \mathcal{P}}{\partial x_i} \tag{2}$$

Here $\mathcal{U}_j$ represents the instantaneous velocity normalized by a characteristic velocity $V_{ch}$ , and $\mathcal{P}$ is physical pressure plus hydrostatic head ($\rho g z$) normalized by $V_{ch}^2$ , where $\rho$ is density, $g$ the gravitational acceleration and $z$ the upward position. The spatial coordinates are made non-dimensional by a characteristic length $L_{ch}$, and time $t$ by $L_{ch}/V_{ch}$. The Reynolds number is $Re = \rho V_{ch} L_{ch}/\mu$, where $\mu$ is the viscosity.

The momentum equation (2) is integrated explicitly. Continuity is satisfied by solving the pressure equation (3), which is obtained by taking the divergence of the momentum equation (2):

$$\frac{\partial^2 \mathcal{P}}{\partial x_i \partial x_i} = \frac{\partial}{\partial x_i}\left[-\frac{\partial (\mathcal{U}_i \mathcal{U}_j)}{\partial x_j} + \frac{1}{Re}\frac{\partial^2 \mathcal{U}_i}{\partial x_j \partial x_j}\right] - \frac{\partial}{\partial t}\frac{\partial \mathcal{U}_i}{\partial x_i} \tag{3}$$

The last term of (3), time derivative of dilation, is discretized in time as:

$$\frac{\partial}{\partial t}\frac{\partial u_i}{\partial x_i} \cong \left(\frac{\partial u_i}{\partial x_i}^{n+1} - \frac{\partial u_i}{\partial x_i}^{n}\right)/\Delta t \tag{4}$$

Velocity divergence at future time *n+1* is assumed nil, and it is made nil at *n=0* by appropriate choice of initial conditions. Exact solutions of the pressure system of equations would produce nil divergence, but round off errors or incomplete iterative solutions generate some dilation; in these cases existing divergence at time *n* is computed to operate as a source term that reduces dilation itself.

This method was used first in the MAC algorithm (Harlow and Welsh, 1965), which popularized the staggered mesh, but is analogously applicable to the collocated and the semi-staggered meshes, leading to numerically distinct continuity and pressure equations. Fig. 2 sketches the two-dimensional continuity cells for the three meshes with the respective velocity components and pressure equation stencils. In all cases pressure is located at the center of the continuity cell, whilst the locations of the velocity components vary.

In the semi-staggered mesh the velocity components are collocated at the continuity cell vertexes. This mesh presented the best performance in comparison with the traditional staggered and collocated meshes in the cavity flow problem when the unrealistic singularities at the moving slid corners were removed (Figueiredo and Oliveira, 2009a, b). Distinct from the traditional meshes, it allows using fully regular grids close to walls parallel to the Cartesian axes, as

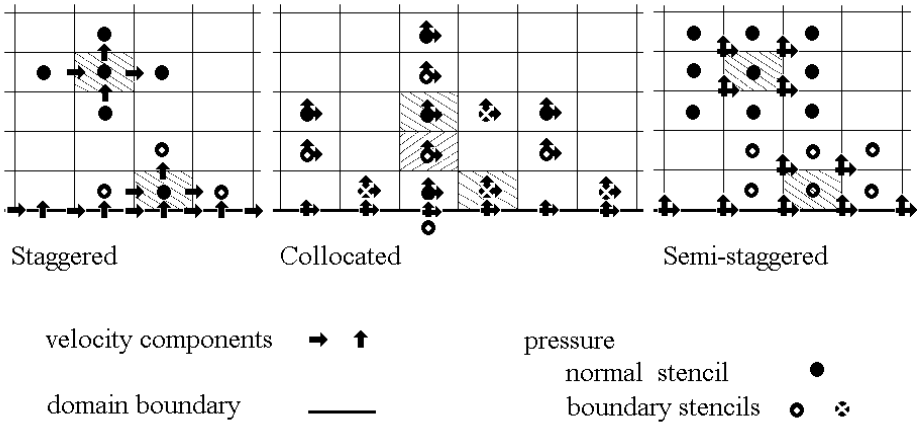


Fig. 2- Continuity cells and corresponding pressure equation stencils for staggered, cell center collocated and semi-staggered meshes.

well as to walls inclined to the axes by adjusting the cell aspect ratio. Due to this geometric flexibility, the semi-staggered mesh was successfully applied to compute the steady-state flow in a channel with a gradual expansion region using entirely regular grid (Nascimento, 2019, Nascimento *et al*., 2020); it would analogously admit rectangular section ducts with contraction or bend.

As shown in fig. 2, the staggered mesh produces the most compact pressure cell, relating each node to its immediate neighbors through the second order central differencing. The collocated mesh produces double-spacing central differencing, forming multiple independent sets of systems of pressure equations whose result presents wiggly aspect. The semi-staggered pressure cell involves immediate and diagonal neighbors; if the mesh is square or cubic it reduces to the diagonal neighbors; wiggly solutions are also possible in both square and rectangular cases.

For simplicity, the numerical representation of the divergence, gradient and Laplacian operators in a 3D semi-staggered mesh will be exemplified by the x-direction part or component. Integer values are adopted for the velocity locations, cell centers require half indexes. The derivative of the velocity component $u = \mathcal{U}_1$ is:

$$\frac{\partial u}{\partial x}_{i-\frac{1}{2},j-\frac{1}{2},k-\frac{1}{2}} \cong \frac{u_{i\ ,j,k}+u_{i\ ,j-1,k}+u_{i\ ,j,k-1}+u_{i\ ,j-1,k-1}-u_{i-1,j,k}-u_{i-1\ ,j-1,k}-u_{i-1\ ,j,k-1}-u_{i-1\ ,j-1,k-1}}{4\Delta x} \tag{5}$$

Analogous relations hold for the other components of the divergences of the velocity and for the momentum flux. The pressure gradient is exemplified as:

$$\frac{\partial \mathcal{P}}{\partial x}_{i,j,k} \cong \frac{\mathcal{P}_{i+\frac{1}{2},j-\frac{1}{2},k-\frac{1}{2}}+\mathcal{P}_{i+\frac{1}{2},j+\frac{1}{2},k-\frac{1}{2}}+\mathcal{P}_{i+\frac{1}{2},j-\frac{1}{2},k+\frac{1}{2}}+\mathcal{P}_{i+\frac{1}{2},j+\frac{1}{2},k+\frac{1}{2}}-\mathcal{P}_{i-\frac{1}{2},j-\frac{1}{2},k-\frac{1}{2}}-\mathcal{P}_{i-\frac{1}{2},j+\frac{1}{2},k-\frac{1}{2}}-\mathcal{P}_{i-\frac{1}{2},j-\frac{1}{2},k+\frac{1}{2}}-\mathcal{P}_{i-\frac{1}{2},j+\frac{1}{2},k+\frac{1}{2}}}{4\Delta x} \tag{6}$$

The resulting Laplacian of the pressure involves 27 nodes and is strongly non diagonally dominant. This was tackled by Santos and Figueiredo (2011) with sub-relaxation factors, but in the present work such complexity is avoided by employing the momentum interpolation procedure analogous to that used by Rhie and Show (1983) with the collocated mesh. It reduces to approaching the pressure second derivative by central differencing:

$$\frac{\partial^2 \mathcal{P}}{\partial x^2}_{i-\frac{1}{2},j-\frac{1}{2},k-\frac{1}{2}} \cong \frac{\mathcal{P}_{i+\frac{1}{2},j-\frac{1}{2},k-\frac{1}{2}}-2\,\mathcal{P}_{i-\frac{1}{2},j-\frac{1}{2},k-\frac{1}{2}}+\mathcal{P}_{i-\frac{3}{2},j-\frac{1}{2},k-\frac{1}{2}}}{\Delta x^2} \tag{7}$$

Yet unpublished results indicate that this approximation has negligible influence on the velocity profile and even on the actual mass conservation for the semi-staggered mesh. The system of pressure equations is solved line by line in alternating direction pseudo-transient approach, usually with twenty iterations per momentum iteration.

The discretization scheme UNIFAES belongs to a class of schemes whose interpolating curve for both advective and diffusive terms is based on the linear equation:

$$u\frac{d\emptyset}{dx} - \frac{1}{Re}\frac{d^2\emptyset}{dx^2} = K \tag{8}$$

that locally approaches the equation of interest, considering $\emptyset$ as the dependent variable, and assuming velocity component $u$ to be locally constant, as well as term $K$, which represents all remaining terms of the equation (2), namely cross-flow, pressure and transient terms. The solution to the approximate equation is:

$$\emptyset = C_1 + C_2 exp(Re.u.x) + \frac{K}{u}x \tag{9}$$

The combined advective and diffusive flux in x-direction results, abstracting the Finite Volume integration on cell face:,

$$\frac{\partial(u\phi)}{\partial x} - Re^{-1}\frac{\partial^2\phi}{\partial x^2} \cong \left(\phi_i - \phi_{i+1}\right)\frac{\pi\left(p_{i+1/2}\right)}{\Delta x} + \left(\phi_i - \phi_{i-1}\right)\frac{\pi\left(p_{i-1/2}\right)}{\Delta x} + \varphi \tag{10}$$

where

$$\pi(p) = \frac{p}{exp(p)-1} \tag{11}$$

$$p_i = Re.u_i.\Delta x \tag{12}$$

$$\varphi = \left[K_{i+1/2}\,\chi\left(p_{i+1/2}\right) - K_{i-1/2}\,\chi\left(p_{i-1/2}\right)\right]\Delta x \tag{13}$$

$$\chi(p) = \frac{\pi(p)-1}{p} + \frac{1}{2} \tag{14}$$

. The best known Finite Volume scheme of this type is the so called Exponential Scheme (Spalding, 1972, Raithby and Torrance, 1974, Patankar, 1980), which neglects the source term $K$, allowing constants $C_1$ and $C_2$ to be determined easily by interpolating between two nodes, but loosing most of the physical realism. The first approaches to include the source term were LOADS, Locally Analytic Differencing Scheme (Wong and Raithby, 1979, Prakash, 1983), which estimates *K* according to the summation of terms it represents, and Flux Spline (Varejão, 1979, Karski *et al.*, 1989), which computes *K* by imposing the continuity of the first derivative of the interpolating curves between all nodes by means of an iterative approach analogous to SIMPLE algorithm for pressure-velocity coupling. Both approaches are complex, and limited applications are found in literature.

The simplest and best succeeded scheme of this type is the Unified Finite Approaches Exponential-type Scheme, UNIFAES (Figueiredo, 1997), which computes the source term *K* of the Finite Volume generating equation by recourse to Allen and Southwell´s (1955) Finite Difference scheme. This first ever exponential scheme determines *K* at any central node by fitting interpolation curve (9) to the central node and the two immediate neighbors, in each direction, resulting:

$$K_i = \left(\phi_i - \phi_{i+1}\right)\Pi^+ + \left(\phi_i - \phi_{i-1}\right)\Pi^- \tag{15}$$

$$\Pi^{\pm} = \frac{\pi\left(\pm p_i\right)}{\Delta x^2} \tag{16}$$

UNIFAES takes the mean of two nodal estimates of *K* by Allen and Southwell's approach to represent the source term between them, i.e.:

$$K_{i\pm1/2} = 0.5\left(K_i + K_{i\pm1}\right) \tag{17}$$

In comparisons with other finite-volume schemes, including Central Differencing, simple Exponential Scheme, Second Order Upwind, QUICK and LOADS, it has shown high stability and superior accuracy in a vast number of cases, including linear tests (Figueiredo, 1997), natural and mixed convection flows in porous media (Figueiredo and Llagostera, 1999, Llagostera and Figueiredo, 2000a, 2000b), and incompressible viscous flows (Figueiredo and Oliveira, 2009a, 2009b, Rodrigues, 2019, Rodrigues *et al*., 2020), presenting second order dominated errors even at moderate meshes. Three dimensional versions of the solver were presented by Santos and Figueiredo (2011) and Nascimento *et al*. (2020), with different approaches with respect to pressure.

The referred solver used Euler integration towards steady state solution. To increase the precision of the time-wise integration for the present work, the first order approach was substituted by a second order predictor-corrector method. The program also received two new routines, one for introducing controlled perturbations to the flow, other for recording instantaneous velocity, vorticity, pressure and shear at prescribed points in the domain to a text-file. This is read afterwards by a program that computes the correlations.

## 3. KINETIC ENERGY – HELICITY TURBULENCE MODEL EQUATIONS

Instantaneous velocity and pressure are decomposed into mean and fluctuating parts, represented by capital and small letters respectively: $\mathcal{U}_i = U_i + u_i$ and $\mathcal{P} = P + p$. The turbulence model is defined by the mean continuity equation (18), the Reynolds averaged Navier-Stokes equations (19), the equation of transport of fluctuating kinetic energy in the form (20) or (21) and the equation of transport of fluctuating helicity (22) (Figueiredo, 2018):

$$\frac{\partial U_j}{\partial x_j} = 0 \tag{18}$$

$$\frac{\partial U_i}{\partial t} = -\frac{\partial (U_i U_j)}{\partial x_j} - \frac{\partial (\overline{u_i u_j})}{\partial x_j} + Re^{-1}\frac{\partial^2 U_i}{\partial x_j \partial x_j} - \frac{\partial P}{\partial x_i} \tag{19}$$

Employing the continuity equation (18), term $Re^{-1}\,\partial^2 U_i/\partial x_j \partial x_j$ of eq. (19) can be alternatively written in terms of mean shear $S_{ij} = 0.5\left(\partial U_i/\partial x_j + \partial U_j/\partial\, x_i\right)$ as $2Re^{-1}\,\partial S_{ij}/\partial x_j$.

The kinetic energy transport equation is obtained by multiplying the instantaneous Navier-Stokes equation by $u_i$. Depending on the form of the viscous term adopted, the energy equation assumes the forms (20) or (21); in most classic textbooks (Tennekes and Lumley, 1972, Hinze, 1975) the last term in Eq. (21) is considered the correct expression of the dissipation work. Because of this, the last term of Eq. (20) is called pseudo-dissipation in present text.

$$\frac{\partial \overline{u_i u_i/2} U_j}{\partial x_j} + \frac{\partial \overline{u_j u_i u_i/2}}{\partial x_j} - Re^{-1}\frac{\partial^2 \overline{u_i u_i/2}}{\partial x_j \partial x_j} = -\frac{\partial \overline{u_j p}}{\partial x_j} - \overline{u_i u_j}\frac{\partial U_i}{\partial x_j} - Re^{-1}\overline{\frac{\partial u_i}{\partial x_j}\frac{\partial u_i}{\partial x_j}}. \tag{20}$$

$$\frac{\partial \overline{u_i u_i/2} U_j}{\partial x_j} + \frac{\partial \overline{u_j u_i u_i/2}}{\partial x_j} - Re^{-1}\frac{\partial \overline{u_i s_{ij}}}{\partial x_j} = -\frac{\partial \overline{u_j p}}{\partial x_j} - \overline{u_i u_j} S_{ij} - Re^{-1}\overline{s_{ij} s_{ij}}. \tag{21}$$

$$\frac{\partial \overline{u_i w_i} U_j}{\partial x_j} - \frac{1}{Re}\frac{\partial^2 \overline{u_i w_i}}{\partial x_j \partial x_j} = \frac{\partial \overline{u_i u_i}/2}{\partial x_j} W_j - \overline{u_i u_j}\frac{\partial W_i}{\partial x_j} - \overline{w_j \frac{\partial p}{\partial x_j}} + \frac{\partial \overline{w_j u_i u_i/2}}{\partial x_j} - \frac{\partial \overline{u_i w_i u_j}}{\partial x_j} - Re^{-1}\overline{\frac{\partial u_i}{\partial x_j}\frac{\partial w_i}{\partial x_j}}. \tag{22}$$

In above expressions $S_{ij}$ is the mean shear rate and $W_i$ is the mean vorticity:

$$S_{ij} = \frac{1}{2}\left(\frac{\partial U_i}{\partial x_j} + \frac{\partial U_j}{\partial x_i}\right) \tag{23}$$

$$W_i = \varepsilon_{ijk}\frac{\partial U_j}{\partial x_k} \tag{24}$$

Complementary algebraic expressions are provided by the relation between the divergence of the Reynolds stress and the velocity-vorticity tensor, Eq. (25) (Tennekes and Lumley, 1972), and the statistical dynamic equation for the velocity-vorticity tensor¨, Eq. (26) (Figueiredo, 2018)

$$\frac{\partial \overline{u_i u_j}}{\partial x_j} = -\varepsilon_{ijk}\overline{u_j w_k} + \frac{\partial \overline{u_j u_j}/2}{\partial x_i} \tag{25}$$

$$\overline{u_i w_k} = S_{kj}\overline{u_i \int_o^t w_j\, dt} + W_j\overline{u_i \int_o^t s_{kj} dt} - \frac{\partial W_k}{\partial x_j}\overline{u_i \int_0^t u_j\, dt} - \overline{u_i \int_0^t \frac{\partial (w_k u_j - w_j u_k)}{\partial x_j} dt} + \frac{1}{Re}\overline{u_i \int_o^t \frac{\partial^2 w_k}{\partial x_j \partial x_j} dt} \tag{26}$$

Statistical dynamic equations can be provided for other terms of the transport equations of kinetic energy and helicity, but are omitted here. On the other side, for completeness of the statistical description of the flow, the correlations of the equation of transport of enstrophy are included: (Tennekes and Lumley, 1972, which use the term "squared vorticity")

$$\frac{\partial U_j \overline{w_i w_i/2}}{\partial x_j} - \nu\frac{\partial^2 \overline{w_i w_i}/2}{\partial x_j \partial x_j} = \overline{w_i s_{ij}} W_j - \overline{w_i u_j}\frac{\partial W_i}{\partial x_j} + \overline{w_i w_j} S_{ij} - \overline{w_i w_j s_{ij}} - \frac{\partial \overline{u_j w_i w_i/2}}{\partial x_j} - \nu\overline{\frac{\partial w_i}{\partial x_j}\frac{\partial w_i}{\partial x_j}}. \tag{27}$$

## 4. INTERPOLATIONS FOR CALIBRATION

Second and forth order central differencing derivations of velocity, vorticity and pressure were implemented in every term of the transport equations of kinetic energy, helicity and enstrophy. Furthermore, the UNIFAES interpolation (Eqs. 10 to 17) for the combined advective and viscous net fluxes is included.
. Since the Navier-Stokes solver is second order in time and space, second order approximations in space and trapezoidal time-wise integration of the statistical dynamic equations offer compatible order of approximation. However, deterioration of the quality of the approximations may be expected for the higher order correlations, suggesting the need for higher, forth order interpolating curves. Approximations employed are exemplified by x-direction derivatives, omitting other indexes when no confusion emerges. Second order approximations are the classic central differencing:

$$\frac{\partial u}{\partial x_i} \cong \frac{u_{i+1}-u_{i-1}}{2\Delta x} \tag{28}$$

$$\frac{\partial^2 u}{\partial x^2{}_i} \cong \frac{u_{i+1}-2u_i+u_{i-1}}{2\Delta x} \tag{29}$$

For divergence form interpolations:

$$\frac{\partial uv}{\partial x}_i \cong \frac{u_{i+1/2}v_{i+1/2}-u_{i-1/2}v_{i-1/2}}{\Delta x} \tag{30}$$

where $u_{i\pm1/2}$ and $v_{i\pm1/2}$ are obtained by linear interpolation from immediate nodes $u_i$ and $u_{i\pm1}$, and $v_i$ and $v_{i\pm1}$. For similar expression with pressure,

$$\frac{\partial up}{\partial x}_i \cong \frac{u_{i+1/2}p_{i+1/2}-u_{i-1/2}p_{i-1/2}}{\Delta x} \tag{31}$$

the required pressure in the momentum cell face center is obtained by interpolation from the values at cell vertexes, for example:

$$p_{i-1/2,j,k} = \frac{p_{i-1/2,j-1/2,k-1/2} + p_{i-1/2,j+1/2,k-1/2} + p_{i-1/2,j-1/2,k+1/2} + p_{i-1/2,j+1/2,k+1/2}}{4} \tag{32}$$

The collocated pressure results from the mean of the eight staggered pressure values around, which equals the mean between $p_{i-1/2,j,k}$ and $p_{i+1/2,j,k}$.

Forth order centered interpolations employed for correlations involving collocated velocities and vorticities are:

$$\frac{\partial u}{\partial x_i} \cong \frac{-u_{i+2}+8u_{i+1}-8u_{i-1}+u_{i-2}}{12\Delta x} \tag{33}$$

$$\frac{\partial^2 u}{\partial x^2{}_i} \cong \frac{-u_{i+2}+16u_{i+1}-30u_i+16u_{i-1}-u_{i-2}}{12\Delta x} \tag{34}$$

For divergence form interpolations:

$$\frac{\partial uv}{\partial x}_i \cong \frac{-u_{i+2}v_{i+2} + 8u_{i+1}v_{i+1} - 8u_{i-1}v_{i-1} + u_{i-2}v_{i-2}}{12\Delta x} \tag{35}$$

Converting pressure from its staggered positions to the velocity positions puts a three-dimensional interpolation problem, which was solved by successive one-dimensional interpolations. The values of pressure and of its first derivative at the velocity positions are interpolated by means of centered third order polynomials according to:

$$p_i \cong \frac{-p_{i+3/2} + 9p_{i+1/2} + 9p_{i-1/2} - p_{i-3/2}}{16} \tag{36}$$

$$\frac{\partial p}{\partial z_i} \cong \frac{-p_{i+3/2}+27p_{i+1/2}-27p_{i-1/2}+p_{i-3/2}}{24\Delta z} \tag{37}$$

Despite based on third order polynomial, these estimates are forth order accurate. Consider velocity node $i,j,k$ at the center of the cube $[i-3/2\,..\,i+3/2\,,\ j-3/2\,..\,j+3/2\,,\ k-3/2\,..\,k+3/2]$ , which contains 64 pressure nodes. For example, pressure on plane $i$ is interpolated for each position $j\pm1/2\,, j\pm3/2\,, k\pm1/2$ and $k\pm3/2$ according to (36). Then, pressure on line $j$ within plane $i$ is interpolated analogously to (36) for each position $k\pm1/2$ and

$k \pm 3/2$ . Finally, pressure at node *i,j,k* is also found by analogous procedure, and the pressure derivative in z direction by means of expression analogous to (37). By distinct routes this method generates six alternative estimates of the pressure at node *i,j,k* and two alternative estimates of the pressure derivative in each direction at that node; the values finally adopted are the means of the six pressure values and of the two derivative values.

## 5. RESULTS

Present computations refer to the Couette flow, as sketched at Fig. 3, with normalized dimensions 5x1x1, having lower and upper impermeable adherent walls with normalized velocity $U_1 = 0$ at $x_2 = 0$ and $U_1 = 1$ at $x_2 = 1$, periodic conditions in span-wise direction $x_3$ , with Reynolds number 600. The inlet and the initial conditions of the problem where simply $\mathcal{U}_i = \mathcal{U}_1 = x_2$. Cubic cells are adopted to prevent numerically produced directional biases. The most refined mesh has been 240x48x48, which is about the limit of the computer or compiler employed. The domain is divided in three regions along its length: the first one fifth admits periodic perturbation, two fifths are used for measuring statistics, and two final fifths are computed with hyper viscosity to suppress perturbations, so that homogeneous Newman exit conditions can be applied.

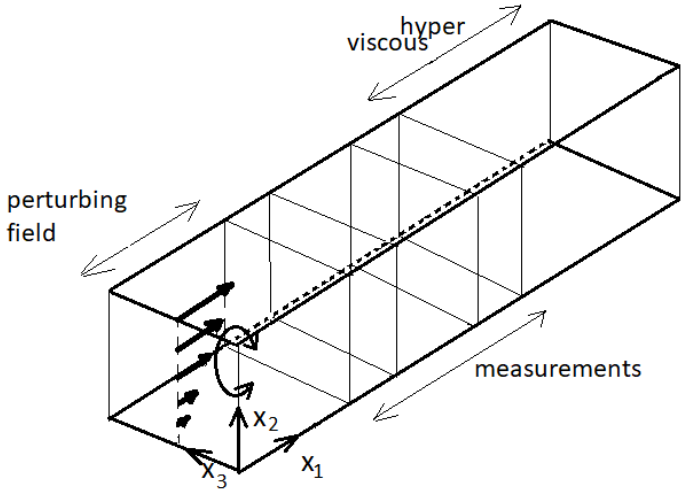


Fig. 3 – Sketch of numerical domain

Perturbations are designed as an oscillating field that enforces rotation around axis $x_3$ with a Gaussian varying strength, centered on node $(x_1^O, x_2^O, x_3^O) = (0.5,0.5,0.5)$, as follows.

$$\boldsymbol{f} = M.sin(2\pi\nu t).exp\left\{-\left[\frac{(x_1-x_1^O)^2}{{\sigma_1}^2}+\frac{(x_2-x_2^O)^2}{{\sigma_2}^2}+\frac{(x_3-x_3^O)^2}{{\sigma_3}^2}\right]\right\}.[-(x_2-x_2^O)\boldsymbol{e}_1+(x_1-x_1^O)\boldsymbol{e}_2] \quad (38)$$

where $\boldsymbol{e}_1$ and $\boldsymbol{e}_2$ are versors, $M = 166.66$, $\sigma_1 = \sigma_2 = 0.2$, $\sigma_3 = 0.4$ and $\nu = 1.0$. Results were obtained after waiting some time for the perturbation to be felt in the whole domain, referring to integration in the interval $25 \leq t \leq 100$, in which the flow is quasi-periodic. Noticeably, it is a smooth profile alternating at unit frequency; it is expected to allow asymptotic convergences to be detected within the refinement levels allowed.

Table 1displays the values of kinetic energy, helicity and enstrophy at 18 selected nodes regularly spaced on planes x=1.5 and x=2.5; the decrease of turbulence levels within these planes clearly reflects high dissipation levels. Central plane z= 0.5 is a plane of symmetry for kinetic energy and enstrophy, and a plane of skew-symmetry for helicity, which is negative at plane z=0.25, positive at plane z=0.75 and practically nil at the central plane z=0.5.

In principle, fluctuating kinetic energy $k = \overline{u_i u_i}/2$ and helicity $h = \overline{u_i w_i}$ allow the definition of time scale $T = k^{1/2}/|h|$ , length scale $L = k/|h|$ , and turbulent Reynolds number $Re_t = k^{3/2}/\upsilon|h|$ . Those time and length scales are also registered in Table 1, showing no relation to the scales of the imposed fluctuation. Since the symmetry plane z = 0.5 presents vanishing helicity, both time and length scales become huge at that plane. Of course a different pattern is to be observed in actual turbulent shear flows, but the possibility of nil helicity seems to prevent the use of referred time and length scales. For the other nodes the estimated time scales are in the range 4 to 9800, while the period of oscillation is unit. Multiplying such period by the mean advective velocity at positions y = 0.25, 0.5 and 0.75, the length scale of the wave would be likewise, i.e., 0.25, 0.5 and 0.75 respectively, while the estimated fluctuating length scale varies in the range 0.02 to 0.1.

Table 1. Turbulence levels at selected nodes

| | | x = 1.5 | | | x = 2.5 | | |
|---|---|---|---|---|---|---|---|
| | | z = 0.25 | z = 0.5 | z = 0.75 | z = 0.25 | z = 0.5 | z = 0.75 |
| y = 0.75 | Node | 7 | 8 | 9 | 16 | 17 | 18 |
| | Kin.Energy | 1.808E-5 | 2.492 E-5 | 1.808E-5 | 6.235 E-6 | 3.300E-6 | 6.235 E-6 |
| | Helicity | -3.260E-4 | -7.173E-15 | 3.260E-4 | -1.900E-4 | 2.101E-13 | 1.900E-4 |
| | Enstrophy | 2.126E-3 | 3.504E-4 | 2.126E-3 | 2.115E-3 | 3.418E-4 | 2.115E-3 |
| | Time scale | 1.30E+1 | 6.96E+11 | 1.30E+1 | 1.31E+1 | 8.64 E+9 | 1.31E+1 |
| | Length scale | 5.55E-2 | 3.47 E+9 | 5.55E-2 | 3.28E-2 | 1.57E+7 | 3.28E-2 |
| y = 0.5 | Node | 4 | 5 | 6 | 13 | 14 | 15 |
| | Kin.Energy | 5.201E-5 | 6.355E-5 | 5.201E-5 | 7.338 E-7 | 1.829 E-7 | 7.338 E-7 |
| | Helicity | -1.588E-3 | 6.780E-12 | 1.588E-3 | -3.272 E-5 | 4.496 E-13 | 3.272 E-5 |
| | Enstrophy | 1.731E-2 | 2.002E-2 | 1.731E-2 | 6.319 E-4 | 1.544 E-4 | 6.319 E-4 |
| | Time scale | 4.54E+0 | 1.18E+9 | 4.54E+0 | 2.62E+1 | 9.51E+8 | 2.62E+1 |
| | Length scale | 3.27E-2 | 9.37E+6 | 3.27E-2 | 2.24E-2 | 4.07 E+5 | 2.24E-2 |
| y = 0.25 | Node | 1 | 2 | 3 | 10 | 11 | 12 |
| | Kin.Energy | 4.706E-8 | 6.497E-8 | 4.706E-8 | 2.995E-9 | 3.127 E-9 | 2.995E-9 |
| | Helicity | -4.708E-7 | -9.250E-17 | 4.708E-7 | -5.569E-9 | -2.194 E-16 | 5.569E-9 |
| | Enstrophy | 6.117 E-6 | 5.656E-6 | 6.117 E-6 | 2.094E-8 | 2.759E-9 | 2.094E-8 |
| | Time scale | 4.61E+2 | 2.76E+12 | 4.61E+2 | 9.83E+3 | 2.55E+11 | 9.83E+3 |
| | Length scale | 9.99E-2 | 1.37E+8 | 9.99E-2 | 5.38E-1 | 1.42E+7 | 5.38E-1 |

### 5.1. Transport equation for fluctuating scalars

Tables 2 to 4 present the terms of the transport equations for kinetic energy, helicity and enstrophy at nodes 4, 5 and 9. Accuracy is evaluated by the unbalance of the equation, by comparing different algebraic forms of most terms, and by comparing second and forth order central differencing representations, as well as the combined advective-viscous term from UNIFAES.

The advection of kinetic energy can be computed in advective form Aa = $U_j \partial\left(\overline{u_\iota u_\iota/2}\right)/\partial x_j$ and in divergence form Ad = $\partial\left(U_j \overline{u_\iota u_\iota/2}\right)/\partial x_j$ , whose equivalence is associated to nil velocity divergence, $\partial U_j/\partial x_j = 0$. Analogous advective and divergence forms exist for the turbulent transport term: Ta = $u_j \partial\left(\overline{u_\iota u_\iota/2}\right)/\partial x_j$ , Td = $\partial\left(\overline{u_j u_\iota u_\iota/2}\right)/\partial x_j$ as well as for the pressure term Pa = $\overline{u_j \partial p}/\partial x_j$ , Pd = $\partial \overline{u_j p}/\partial x_j$ . As seen in Table 2, advective and divergence forms of the advective term present four digit equality, corresponding forms for turbulent transport term differ up to about 2% and for pressure term differ up to 8%. Differences between second and forth order central differencings are less than 0.1%. in the case of advective transport, achieve 5% for turbulent transport and 9% for pressure.

In deriving the energy equation in the form (20), after the scalar multiplication of the momentum equation (2) by the velocity, the viscous term Vu= $Re^{-1} u_i(\partial^2 u_i)/\left(\partial x_j \partial x_j\right)$ is decomposed as diffusion Df= $Re^{-1}\, \partial^2(\overline{u_\iota u_\iota/2})/\partial x_j \partial x_j$ minus pseudo-dissipation Du= $Re^{-1}\left(\partial u_i/\partial x_j\right)\left(\partial u_i/\partial x_j\right)$. As reported in Table 2, for all these terms, differences between second and forth order are generally about unit, but achieve 4%. The differences between the global viscous term and the combination of its components are roughly 3% for the second order approximations and below 0.2% for the forth order interpolations.

For the alternative form (21) of the energy equation, the viscous term Vs= $Re^{-1} u_i \partial s_{ij}/\partial x_j$ is decomposed as transport of energy by viscous stresses Ts= $Re^{-1}\, \partial\left(u_i s_{ij}\right)/\partial x_j$ minus dissipation Ds= $Re^{-1} s_{ij} s_{ij}$. Differences between second and forth order approximations achieve 7.6%. The forth order interpolations also show expressively greater coherence between the viscous terms.

The interpolation with Unifies agrees within negligible differences with the combination of advective and viscous terms by the central difference schemes, particularly the second order. The two forms of the production term, PS = -$\overline{u_j} S_{ij}$ and PU = - $\overline{u_\iota u_j}\, \partial U_i/\partial x_j$ , differ at the level of round-off error. Notice the negative production of fluctuating kinetic energy as an example of lack of correspondence between the present fluctuating laminar flow and the physics of turbulence.

Because the flow is not rigorously periodic, some difference exists between the kinetic energy at the beginning and the end of the integration period, although it is a multiple of the period of oscillation. These differences divided by the

Table 2. Statistics of kinetic energy transport equation at selected nodes

| Term | Node 4 | | | Node 5 | | | Node 9 | | |
|---|---|---|---|---|---|---|---|---|---|
| | $2^{nd}$ order | $4^{th}$ order | ≠% | $2^{nd}$ order | $4^{th}$ order | ≠% | $2^{nd}$ order | $4^{th}$ order | ≠%. |
| Aa | -8.129E-5 | -8.127E-5 | 0.0 | -1.277E-4 | -1.276E-4 | 0.1 | -1.284E-5 | -1.284E-5 | 0.0 |
| Ad | -8.129E-5 | -8.127E-5 | 0.0 | -1.277E-4 | -1.276E-4 | 0.1 | -1.284E-5 | -1.284E-5 | 0.0 |
| Aa≠Ad | 0.0% | 0.0% | | 0.0% | 0.0% | | 0.0% | 0.0% | |
| Ta | -3.562E-8 | -3.608E-8 | 1.3 | 6.200E-8 | 6.035E-8 | 2.7 | -3.261E-8 | -3.312E-8 | 1.5 |
| Td | -3.486E-8 | -3.606E-8 | 3.3 | 6.215E-8 | 5.900E-8 | 5.1 | -3.333E-8 | -3.339E-8 | 0.2 |
| Ta≠Td | 2.1% | 0.1% | | 0.2% | 2.2% | | 2.2% | 0.8% | |
| Pa | -1.197E-5 | -1.217E-5 | 1.6 | 2.612E-6 | 2.572E-6 | 1.5 | 1.112E-5 | 1.114E-5 | 0.2 |
| Pd | -1.207E-5 | -1.215E-5 | 0.7 | 2.438E-6 | 2.705E-6 | 9.9 | 1.022E-5 | 1.084E-5 | 5.7 |
| Pa≠Pd | 0.8% | 0.2% | | 6.7% | 4.9% | | 8.1% | 2.7% | |
| Df | -6.054E-6 | -6.114E-6 | 1.0 | -6.031E-6 | -6.126E-6 | 1.6 | 4.098E-6 | 4.123E-6 | 0.6 |
| Du | 5.531E-5 | 5.770E-5 | 0.7 | 6.616E-5 | 6.897E-5 | 4.1 | 9.725E-6 | 9.853E-6 | 1.3 |
| Vu | -6.305E-5 | -6.390E-5 | 1.3 | -7.421E-5 | -7.521E-5 | 1.3 | -5.799E-6 | -5.730E-6 | 1.2 |
| Vu≠Df-Du | 2.7% | 0.1% | | 2.7% | 0.2% | | 3.0% | 0.0% | |
| Ts | -8.226E-6 | -8.725E-6 | 5.7 | -6.390E-6 | -6.918E-6 | 7.6 | 6.496E-6 | 6.882E-6 | 5.6 |
| Ds | 5.292E-5 | 5.506E-5 | 3.9 | 6.560E-5 | 6.807E-5 | 3.6 | 1.236E-5 | 1.263E-5 | 2.1 |
| Vs | -6.049E-5 | -6.371E-5 | 5.1 | -7.096E-5 | -7.489E-5 | 5.2 | -6.070E-6 | -5.762E-6 | 5.1 |
| Vs≠Ts-Ds | 0.1% | 0.1% | | 1.4% | 0.0% | | 3.4% | 0.2% | |
| Vs≠Vu | 4.1% | 0.3% | | 4.3% | 0.4% | | 4.5% | 0.6% | |
| Un | -7.521E-5 | | | -1.215E-4 | | | -1.694E-5 | | |
| Un≠Ad-Df | 0.0% | 0.1% | | 0.1% | 0.0% | | 0.0% | 0.1% | |
| PU | -3.341E-5 | -3.343E-5 | 0.1 | -5.472E-5 | -5.474E-5 | 0.0 | -1.991E-6 | -1.991E-6 | 0.0 |
| PS | -3.341E-5 | -3.343E-5 | 0.1 | -5.472E-5 | -5.474E-5 | 0.0 | -1.991E-6 | -1.991E-6 | 0.0 |
| PU≠PS | 0.0% | 0.0% | | 0.0% | 0.0% | | 0.0% | 0.0% | |
| Var. KinEn. | 6.971E-8 | | | 1.568E-7 | | | 1.417E-8 | | |
| Eq. (20) | 1.492E-6 | 3.770E-6 | | 1.928E-6 | 4.895E-6 | | 1.887E-6 | 2.003E-6 | |
| Unbalance | 1.8 / 1.4 | 4.6 / 3.6 | | 1.5 / 1.3 | 3.8 / 3.2 | | 14.7 / 9.4 | 15.6 / 9.9 | |
| Eq. (21) | 1.272E-6 | 3.746E-6 | | 1.725E-6 | 4.787E-6 | | 2.127E-6 | 1.708E-6 | |
| Unbalance | 1.6 / 1.2 | 4.6 / 3.6 | | 1.4 / 1.1 | 3.8 / 3.1 | | 16.6 / 9.6 | 13.3 / 9.1 | |

integration period are reported (Var.KinEn) as estimates of possible influence of this factor upon the computed means, being sensibly small.

The two last lines of Table 2 present the unbalances of equations (20) and (21), performed with the advective forms of the advective, turbulent transport and pressure terms; the divergence form unbalances are very close. In each space, the value of the residual is presented above; below two percentages are presented: first, the percentage relative to the maximum term of the balance equation, second the percentage relative to the square root of the sum of the squares of all terms of each equation. Unbalances are small for nodes 4 and 5, but achieve two digits for node 9.

The transport equation unbalances favored the second order interpolation in five among six comparisons of the two last lines of Table 2. This is not a general situation, quite the opposite: considering the 18 nodes, the mean unbalance of Eqs. (20) and (21) were 7.1% and 7.8% respectively for second order interpolations but only 6.0% and 6.1% respectively for forth order interpolations. This is also true for helicity and enstrophy, whose mean unbalances are 12.2% and 6.1% respectively for second order interpolations and 12.0% and 3.7% for forth order interpolations.

Irrespective of such lack of generalization, the superiority of the second order residuals in most comparisons of Table 2 is in apparent contradiction with other comparisons of the same Table. The forth order interpolations produced more coherent results than second order interpolation in 14 among 18 comparisons between advective and divergence forms or between different forms of the viscous term; both orders matched with 0.0% discrepancies in 3 cases and the second order was more coherent in only one case of turbulent transport.

This contradiction regarding the superiority of second or forth order interpolations seems to indicate independence between the unbalance of equations and the discrepancies between alternative algebraic forms; the unbalance seems to represent an error which is not detectable by the comparisons between algebraic forms. Indeed, the residual may be much greater than the summation of the discrepancies of the various terms would suggest. For instance, the greatest discrepancy found in node 4 with second order interpolation is related to the difference of viscous terms Df-Du compared with Vu, which is 2.7% of 6.3E-5, equal to 1.7E-6, which is capable of explaining the unbalance; however, with forth order approximations in the same node 4, the residual is much greater than the summation of estimates of discrepancies. Similar phenomena occurs with nodes 5 and 9.

Table 3. Statistics of helicity transport equation at selected nodes

| Term | Node 4 | | | Node 5 | | | Node 9 | | |
|---|---|---|---|---|---|---|---|---|---|
| | 2nd order | 4th order | ≠% | 2nd order | 4th order | ≠% | 2nd order | 4th order | ≠% |
| Aa | 1.955E-3 | 1.986E-3 | 1.6 | -3.620E-12 | -3.671E-12 | 1.4 | -1.376E-5 | -1.413E-5 | 2.6 |
| Ad | 1.955E-3 | 1.986E-3 | 1.6 | -3.628E-12 | -3.672E-12 | 1.2 | -1.376E-5 | -1.413E-5 | 2.6 |
| Aa≠Ad | 0.0% | 0.0% | | 0.2% | 0.0% | | 0.0% | 0.0% | |
| Ta | 1.538E-6 | 1.631E-6 | 5.7 | 5.520E-14 | 6.020E-14 | 8.3 | -9.224E-7 | -9.638E-7 | 4.3 |
| Td | 1.465E-6 | 1.604E-6 | 8.7 | 5.650E-14 | 6.069E-14 | 6.9 | -9.352E-7 | -9.669E-7 | 3.3 |
| Ta≠Td | 4.7% | 1.7% | | 2.3% | 0.8% | | 1.4% | 0.3% | |
| Pa | 2.400E-4 | 2.473E-4 | 3.0 | -3.532E-12 | -3.638E-12 | 2.9 | 2.071E-5 | 2.644E-5 | 21.7 |
| Pd | 2.419E-4 | 2.479E-4 | 2.4 | -3.513E-12 | -3.637E-12 | 3.4 | 1.929E-5 | 2.644E-5 | 27.0 |
| Pa≠Pd | 0.8% | 0.2% | | 0.5% | 0.0% | | 6.9% | 0.0% | |
| Df | 2.506E-4 | 2.631E-4 | 4.8 | -2.414E-12 | -2.540E-12 | 5.0 | 1.478E-4 | 1.504E-4 | 1.7 |
| Ds | -2.078E-3 | -2.189E-3 | 5.1 | 5.994E-12 | 6.297E-12 | 4.8 | 1.739E-4 | 1.713E-4 | 1.5 |
| Vu | 2.352E-3 | 2.457E-3 | 4.3 | -8.465E-12 | -8.847E-12 | 4.3 | -2.767E-5 | -2.072E-5 | 25.1 |
| Vu≠Df-Ds | 1.0% | 0.2% | | 0.7% | 0.1% | | 5.7% | 0.9% | |
| Un | 1.706E-3 | 1.724E-3 | 1.0 | -1.222E-12 | -1.181E-12 | 3.3 | -1.626E-4 | -1.647E-4 | 1.3 |
| Un≠Ad-Af | 0.1% | 0.1% | | 0.7% | 4.1% | | 0.6% | 0.1% | |
| P1a | -1.210E-4 | -1.213E-4 | 0.2 | 6.184E-13 | 6.246E-13 | 1.0 | 4.957E-5 | 4.971E-5 | 0.3 |
| P1d | -1.210E-4 | -1.213E-4 | 0.2 | 6.204E-13 | 6.248E-13 | 0.7 | 4.959E-5 | 4.971E-5 | 0.3 |
| P1a≠P1d | 0.0% | 0.0% | | 0.3% | 0.0% | | 0.0% | 0.0% | |
| P2 | -8.803E-6 | -9.156E-6 | 3.9 | -2.378E-13 | -2.331E-13 | 2.0 | -5.527E-7 | -6.148E-7 | 10.1 |
| PT1 | 3.667E-7 | 3.644E-7 | 0.6 | 1.534E-14 | 1.694E-14 | 9.4 | -4.498E-7 | -4.733E-7 | 5.0 |
| PT2 | 3.531E-7 | 3.535E-7 | 0.1 | 1.525E-14 | 1.689E-14 | 9.7 | -4.507E-7 | -4.733E-7 | 4.8 |
| PT3 | 3.618E-7 | 3.599E-7 | 0.5 | 1.536E-14 | 1.700E-14 | 9.6 | -4.571E-7 | -4.746E-7 | 4.7 |
| ≠PT1..3 | 3.7% | 3.0% | | 0.7% | 0.6% | | 1.6% | 0.3% | |
| Var. Helic. | 1.201E-7 | | | -1.783E-15 | | | 5.073E-8 | | |
| Equation Unbalance | -1.977E-5<br>1.0 / 0.7 | -1.059E-4<br>4.8 / 3.6 | | 4.391E-13<br>7.3 / 5.3 | 7.134E-13<br>11.3 / 8.3 | | -1.754E-5<br>10.1 / 7.5 | -1.764E-5<br>10.3 / 7.5 | |

Table 4. Statistics of enstrophy transport equation at selected nodes

| Term | Node 4 | | | Node 5 | | | Node 9 | | |
|---|---|---|---|---|---|---|---|---|---|
| | 2nd order | 4th order | ≠% | 2nd order | 4th order | ≠% | 2nd order | 4th order | ≠% |
| Aa | -2.269E-2 | -2.342E-2 | 3.1 | -3.832E-2 | -3.975E-2 | 3.6 | 1.333E-3 | 1.337E-3 | 0.3 |
| Ad | -2.269E-2 | -2.342E-2 | 3.1 | -3.832E-2 | -3.975E-2 | 3.6 | 1.333E-3 | 1.337E-3 | 0.3 |
| Aa≠Ad | 0.0% | 0.0% | | 0.0% | 0.0% | | 0.0% | 0.0% | |
| Ta | -4.128E-5 | -4.490E-5 | 8.1 | -1.614E-6 | -2.588E-6 | 37.6 | -7.601E-6 | -7.684E-6 | 1.1 |
| Td | -3.905E-5 | -4.397E-5 | 11.2 | 7.760E-6 | 1.516E-6 | 80.5 | -7.849E-6 | -7.679E-6 | 2.2 |
| Ta≠Td | 5.4% | 2.1% | | 120.8% | 158.6% | | 3.2% | 0.1% | |
| Df | -1.842E-3 | -2.006E-3 | 8.2 | -1.454E-3 | -1.610E-3 | 9.7 | 1.565E-3 | 1.587E-3 | 1.4 |
| Ds | 2.584E-2 | 2.889E-2 | 10.6 | 3.064E-2 | 3.437E-2 | 10.8 | 1.943E-3 | 2.011E-3 | 3.4 |
| Vw | -2.869E-2 | -3.097E-2 | 7.4 | -3.331E-2 | -3.607E-2 | 7.7 | -4.402E-4 | -4.239E-4 | 3.7 |
| Vw≠Df-Dw | 3.5% | 0.2% | | 3.7% | 0.3% | | 14.1% | 0.0% | |
| Un | -2.084E-2 | -2.140E-2 | 2.6 | -3.685E-2 | -3.811E-2 | 3.3 | -2.316E-4 | -2.533E-4 | 8.6 |
| Un≠Ad-Df | 0.0% | 0.1% | | 0.0% | 0.1% | | 0.2% | 1.3% | |
| P1 | 1.498E-4 | 1.624E-4 | 7.8 | 2.008E-4 | 2.254E-4 | 10.9 | -1.061E-5 | -1.047E-5 | 1.4 |
| P2 | 4.771E-3 | 4.929E-3 | 3.2 | -4.000E-4 | -4.207E-4 | 4.9 | 1.370E-3 | 1.368E-3 | 0.1 |
| P3 | 5.262E-3 | 5.244E-4 | 0.3 | -5.986E-3 | -6.151E-3 | 2.7 | 2.444E-4 | 2.559E-4 | 4.5 |
| PT | 3.706E-6 | 4.966E-6 | 25.4 | 1.089E-4 | 1.185E-4 | 8.1 | -1.392E-6 | -1.593E-6 | 12.6 |
| Var. Enstr. | -2.167E-5 | | | 4.434E-5 | | | 8.809E-7 | | |
| Equation Unbalance | -1.966E-4<br>0.8 / 0.6 | 2.143E-3<br>7.4 / 5.7 | | 2.541E-4<br>0.7 / 0.5 | 2.914E-3<br>7.3 / 5.5 | | 7.907E-5<br>5.5 / 2.5 | 1.206E-4<br>6.0 / 3.8 | |

Table 3 refers to helicity. Advective and turbulent transport terms of helicity in advective and divergence forms are entirely analogous to energy: Aa = $U_j\partial(\overline{u_\iota w_\iota})/\partial x_j$ , Ad = $\partial\left(U_j\overline{u_\iota w_\iota}\right)/\partial x_j$ , Ta = $u_j\partial(u_i w_i)/\partial x_j$ , Td = $\partial(\overline{u_\iota w_\iota})/\partial x_j$ .

Two forms of the pressure term are Pa = $\overline{w_j\partial p}/\partial x_j$ are Pd = $\partial\overline{w_j p}/\partial x_j$. As shown in Table 3, the differences between advective and divergence forms are generally small, except for second order estimate of the pressure term, while differences between second and forth order central differencing approximations of those terms are generally higher than those of kinetic energy, particularly in node 9.

Viscous terms are diffusion Df = $\partial\overline{\left(w_j u_\iota u_\iota/2\right)}/\partial x_j$, dissipation Ds = $Re^{-1}\left(\partial u_i/\partial x_j\right)\left(\partial w_i/\partial x_j\right)$ and total viscous term Vu = $Re^{-1}\left[u_i(\partial^2 w_i)/\left(\partial x_j\partial x_j\right) + w_i(\partial^2 u_i)/\left(\partial x_j\partial x_j\right)\right]$ , which show good consistency between themselves, as measured by the difference between Vu and Df-Ds (Vu≠Df-Ds). .

There is expressive agreement between UNIFAES and both central differencing representations of the advective and viscous net flux.

There are two production terms related to interaction of fluctuating flow with mean flow; the first term was computed in the forms P1a = $W_j\partial\,(\overline{u_\iota w_\iota})/\partial x_j$ and P1d = $\partial\,\left(\overline{u_\iota w_\iota}W_j\right)/\partial x_j$ ; the second term was computed only as P2 = $\overline{u_\iota u_j}\,\partial W_i/\partial x_j$. P1a or P1d is numerically relevant and presents small differences between these two forms and between second and forth order discretizations, whilst P2 is minute and show higher relative discrepancies, particularly for node 9. Finally there is one turbulent production term, numerically small, which assumes the alternative forms PT1 = $\overline{u_\iota w_j s_{\iota j}}$ , PT2 = $\overline{w_j\,\partial(u_\iota u_\iota/2)/\partial x_j}$ and PT3 = $\partial\overline{\left(w_j u_\iota u_\iota/2\right)}/\partial x_j$, which differ by 3.7% at most; forth order central differences shows more coherent results than second order ones.

The balance of the helicity transport equation is accurate in node 4 with second order interpolation, but the unbalances achieve the order of 10% in nodes 5 and 9.

The small unbalance of node 4 with second order could be explained by the discrepancy observed in the difference of viscous terms compared to global viscous term. For all other cases, the unbalances are much greater than the summation of specific discrepancies would suggest.

Table 4 concerns the transport of enstrophy, whose advective and turbulent transport terms are analogous to those of kinetic energy, with minute differences between advective or divergence forms or between different discretizations of advection term; turbulent transport term presents small relative errors except for node 5, in which the turbulent transport term is four orders of magnitude smaller than the dominant terms.

The viscous terms Vw = $Re^{-1}\,w_i(\partial^2 w_i)/\left(\partial x_j\partial x_j\right)$ is decomposed into diffusion Df = $Re^{-1}\,\partial^2\overline{(w_\iota w_\iota/2)}/\partial x_j\partial x_j$ minus dissipation Dw = $Re^{-1}\left(\partial w_i/\partial x_j\right)\left(\partial w_i/\partial x_j\right)$. Analogous to previous cases, the consistency of the relation Vw=Df-Dw is very good using the forth order interpolation, buy is poorer using second order, particularly for node 9. The results of UNIFAES match the combined advective-viscous results with either second and forth order central differencing.

There are three production terms relative to interactions between fluctuating and mean flows, P1= $\overline{w_\iota u_j}\,\partial W_i/\partial x_j$ , P2= $\overline{w_\iota w_j}S_{ij}$, and P3= $\overline{w_\iota s_{\iota j}}W_j$ , and one production term due to fluctuating flow, PT= $\overline{w_\iota w_j s_{\iota j}}$ . P2 and P3 are numerically relevant, P1 is predictably small because the unperturbed main flow presents no vorticity derivative, the fluctuating production PT is also small. The error of these terms can not be evaluated by comparison with alternative forms, comparisons between second and forth order discretizations indicate the numerically important term P3 to present great errors in nodes 4 and 9.

Since the mesh could not be refined significantly more, a mesh refinement study was performed using coarser grids, with meshes 120x24x23 and 160x32x32, as show in Tables 6 to 8 for node 4. Prior to that, Table 5 gives a global appreciation of the evolution of turbulence properties with refinement, presenting kinetic energy, helicity, enstrophy and the Reynolds stress tensor normalized by energy. Evolution is not equal for properties and for nodes. Kinetic energy increases with refinement for nodes 4 and 5 but oscillates for node 9; helicity oscillates in nodes 4 and 9 and decrease in node 5; enstrophy increases with refinement for node 4 but oscillates for nodes 5 and 9; normalized Reynolds stress components may increase, decrease or oscillate. Occurrence of oscillations implies that necessarily the sample of data is not fully determined by the smallest order term of the error; at least the rougher refinement is surely affected by higher order terms. The evolution between the two more refined results is more likely to reveal asymptotic tendencies.

Tables 6 to 8 consider the terms of kinetic energy, helicity and enstrophy transport equations for the meshes 120x24x24 , 160x32x32 and 240x48x48, for node 4 only. With one exception, the discrepancies, either between different orders of interpolation or between different algebraic forms, decrease with refinement; the exception is the difference between second and forth order discretizations of the advective form of the turbulent advection term of the transport of kinetic energy, in which the intermediate mesh presents the smallest error; this affects a term of minor quantitative relevance. The unbalances appear to show a general tendency of decrease with refinement, with some exceptions or irregularities. Considering the balances to depend on several terms, somewhat erratic evolution with refinement can be understood.

Table 5 – Kinetic energy and normalized Reynolds tensor in node 4 for varying mesh refinement

| Node | Property | 120 x 24 x 24 | | | 160 x 32 x 32 | | | 240 x 48 x 48 | | |
|---|---|---|---|---|---|---|---|---|---|---|
| 4 | Kinetic energy | 5.474E-5 | | | 5.454E-5 | | | 5.201E-5 | | |
| | Helicity | - 1.515E- 3 | | | -1.605E-3 | | | -1.588E-3 | | |
| | Enstrophy | 1.573E-2 | | | 1.717E-2 | | | 1.731E-2 | | |
| | Normalized Reynolds tensor | 0.805 | 0.643 | 0.111 | 0.788 | 0.637 | 0.000 | 0.773 | 0.632 | 0.011 |
| | | 0.643 | 0.726 | 0.324 | 0.637 | 0.720 | 0.326 | 0.632 | 0.720 | 0.330 |
| | | 0.111 | 0.324 | 0.469 | 0.000 | 0.326 | 0.492 | 0.011 | 0.330 | 0.508 |
| 5 | Kinetic energy | 6.968E-5 | | | 6.773E-5 | | | 6.355E-5 | | |
| | Helicity | 3.684E-11 | | | 2.325E-11 | | | 6.780E-12 | | |
| | Enstrophy | 1.939E-2 | | | 2.040E-2 | | | 2.002E-2 | | |
| | Normalized Reynolds tensor | 0.826 | 0.837 | 0.000 | 0.808 | 0.839 | 0.000 | 0.791 | 0.838 | 0.000 |
| | | 0.837 | 1.174 | 0.000 | 0.839 | 1.192 | 0.000 | 0.838 | 1.209 | 0.000 |
| | | 0.000 | 0.000 | 0.000 | 0.000 | 0.000 | 0.000 | 0.000 | 0.000 | 0.000 |
| 9 | Kinetic energy | 1.806E-5 | | | 1.836E-5 | | | 1.808E-5 | | |
| | Helicity | 3.154E-4 | | | 3.267E-4 | | | 3.260E-4 | | |
| | Enstrophy | 2.070E-3 | | | 2.134E-3 | | | 2.126E-3 | | |
| | Normalized Reynolds tensor | 0.293 | -0.151 | -0.406 | 0.293 | -0.126 | -0.396 | 0.293 | -0.110 | -0.387 |
| | | -0.151 | 1.043 | 0.521 | -0.126 | 1.043 | 0.528 | -0.110 | 1.045 | 0.532 |
| | | -0.406 | 0.521 | 0.664 | -0.396 | 0.528 | 0.664 | -0.387 | 0.532 | 0.662 |

Table 6. Statistics of kinetic energy transport equation for node 4 with varying refinements

| Term | Mesh 120 x 24 x 24 | | | Mesh 160 x 32 x 32 | | | Mesh 240 x 48 x 48 | | |
|---|---|---|---|---|---|---|---|---|---|
| | $2^{nd}$ order | $4^{th}$ order | ≠% | $2^{nd}$ order | $4^{th}$ order | ≠% | $2^{nd}$ order | $4^{th}$ order | ≠% |
| Aa | -8.020E-5 | -8.013E-5 | 0.1 | -8.252E-5 | -8.248E-5 | 0.0 | -8.129E-5 | -8.127E-5 | 0.0 |
| Ad | -8.021E-5 | -8.013E-5 | 0.1 | -8.252E-5 | -8.248E-5 | 0.0 | -8.129E-5 | -8.127E-5 | 0.0 |
| Aa≠Ad | 0.0% | 0.0% | | 0.0% | 0.0% | | 0.0% | 0.0% | |
| Ta | -2.017E-8 | -1.912E-8 | 5.2 | -2.877E-8 | -2.845E-8 | 1.1 | -3.562E-8 | -3.608E-8 | 1.3 |
| Td | -1.998E-8 | -2.150E-8 | 7.1 | -2.782E-8 | -2.904E-8 | 4.2 | -3.486E-8 | -3.606E-8 | 3.3 |
| Ta≠Td | 1.0% | 11.1% | | 3.3% | 2.0% | | 2.1% | 0.1% | |
| Pa | -1.604E-5 | -1.685E-5 | 4.8 | -1.400E-5 | -1.446E-5 | 3.2 | -1.197E-5 | -1.217E-5 | 1.6 |
| Pd | -1.547E-5 | -1.678E-5 | 7.8 | -1.399E-5 | -1.444E-5 | 3.1 | -1.207E-5 | -1.215E-5 | 0.7 |
| Pa≠Pd | 3.6% | 0.4% | | 0.1% | 0.1% | | 0.8% | 0.2% | |
| Df | -6.963E-6 | -7.271E-6 | 4.2 | -6.706E-6 | -6.867E-6 | 2.3 | -6.054E-6 | -6.114E-6 | 1.0 |
| Du | 5.061E-5 | 5.860E-5 | 13.6 | 5.495E-5 | 6.013E-5 | 8.6 | 5.531E-5 | 5.770E-5 | 0.7 |
| Vu | -6.409E-5 | -6.731E-5 | 4.8 | -6.553E-5 | -6.748E-5 | 2.9 | -6.305E-5 | -6.390E-5 | 1.3 |
| Vu≠Df-Du | 10.2% | 2.1% | | 5.9% | 0.7% | | 2.7% | 0.1% | |
| Ts | -7.834E-6 | -9.552E-6 | 18.0 | -8.420E-6 | -9.545E-6 | 11.8 | -8.226E-6 | -8.725E-6 | 5.7 |
| Ds | 4.877E-5 | 5.586E-5 | 12.7 | 5.267E-5 | 5.729E-5 | 8.1 | 5.292E-5 | 5.506E-5 | 3.9 |
| Vs | -5.457E-5 | -6.448E-5 | 15.4 | -5.971E-5 | -6.648E-5 | 10.2 | -6.049E-5 | -6.371E-5 | 5.1 |
| Vs≠Ts-Ds | 3.7% | 1.4% | | 2.3% | 0.5% | | 0.1% | 0.1% | |
| Vs≠Vu | 14.9% | 4.2% | | 9.7% | 1.5% | | 4.1% | 0.3% | |
| Un | -7.316E-5 | | | -7.577E-5 | | | -7.521E-5 | | |
| Un≠Ad-Df | 0.1% | 0.4% | | 0.0% | 0.0% | | 0.0% | 0.1% | |
| PU | 3.575E-5 | 3.580E-5 | 0.1 | -3.532E-5 | -3.535E-5 | 0.1 | -3.341E-5 | -3.343E-5 | 0.1 |
| PS | 3.575E-5 | 3.580E-5 | 0.1 | -3.532E-5 | -3.535E-5 | 0.1 | -3.341E-5 | -3.343E-5 | 0.1 |
| PU≠PS | 0.0% | 0.0% | | 0.0% | 0.0% | | 0.0% | 0.0% | |
| Var. KinEn. | 5.489E-7 | | | 3.890E-7 | | | 6.971E-8 | | |
| Eq. (20) Unbalance | -2.931E-6<br>3.7 / 2.9 | 4.672E-6<br>5.8 / 4.4 | | 4.357E-7<br>0.5 / 0.4 | 5.380E-6<br>6.5 / 4.9 | | 1.492E-6<br>1.8 / 1.4 | 3.770E-6<br>4.6 / 3.6 | |
| Eq. (21) Unbalance | -3.898E-6<br>4.9 / 3.8 | 4.214E-6<br>5.3 / 4.0 | | -1.332E-7<br>0.2 / 0.2 | 5.220E-6<br>6.3 / 4.8 | | 1.272E-6<br>1.6 / 1.2 | 3.746E-6<br>4.6 / 3.6 | |

Table 7. Statistics of helicity transport equation for node 4 with varying refinements

| | Mesh 120 x 24 x 24 | | | Mesh 160 x 32 x 32 | | | Mesh 240 x 48 x 48 | | |
|---|---|---|---|---|---|---|---|---|---|
| | $2^{nd}$ order | $4^{th}$ order | ≠% | $2^{nd}$ order | $4^{th}$ order | ≠% | $2^{nd}$ order | $4^{th}$ order | ≠% |
| Aa | 1.728E-3 | 1.824E-3 | 5.3 | 1.898E-3 | 1.961E-3 | 3.2 | 1.955E-3 | 1.986E-3 | 1.6 |
| Ad | 1.728E-3 | 1.824E-3 | 5.3 | 1.898E-3 | 1.961E-3 | 3.2 | 1.955E-3 | 1.986E-3 | 1.6 |
| Aa≠Ad | 0.0% | 0.0% | | 0.0% | 0.0% | | 0.0% | 0.0% | |
| Ta | 9.521E-7 | 1.146E-6 | 16.9 | 1.283E-6 | 1.432E-6 | 10.4 | 1.538E-6 | 1.631E-6 | 5.7 |
| Td | 8.641E-7 | 1.139E-6 | 24.1 | 1.170E-6 | 1.389E-6 | 15.8 | 1.465E-6 | 1.604E-6 | 8.7 |
| Ta≠Td | 9.2% | 0.4% | | 8.8% | 3.0% | | 4.7% | 1.7% | |
| Pa | 2.859E-4 | 3.150E-4 | 9.2 | 2.671E-4 | 2.844E-4 | 6.1 | 2.400E-4 | 2.473E-4 | 3.0 |
| Pd | 2.886E-4 | 3.227E-4 | 10.6 | 2.703E-4 | 2.874E-4 | 5.9 | 2.419E-4 | 2.479E-4 | 2.4 |
| Pa≠Pd | 1.0% | 2.4% | | 1.2% | 1.0% | | 0.8% | 0.2% | |
| Df | 2.389E-4 | 2.796E-4 | 14.6 | 2.573E-4 | 2.846E-4 | 9.6 | 2.506E-4 | 2.631E-4 | 4.8 |
| Ds | -1.755E-3 | -2.087E-3 | 15.9 | -2.007E-3 | -2.238E-3 | 10.3 | -2.078E-3 | -2.189E-3 | 5.1 |
| Vu | 2.090E-3 | 2.427E-3 | 13.9 | 2.320E-3 | 2.544E-3 | 8.8 | 2.352E-3 | 2.457E-3 | 4.3 |
| Vu≠Df-Ds | 4.6% | 2.5% | | 2.4% | 0.8% | | 1.0% | 0.2% | |
| Un | 1.493E-3 | 1.552E-3 | 13.9 | 1.642E-3 | 1.680E-3 | 2.3 | 1.706E-3 | 1.724E-3 | 1.0 |
| Un≠Ad-Af | 0.3% | 0.5% | | 0.1% | 0.2% | | 0.1% | 0.1% | |
| P1a | -1.378E-4 | -1.390E-4 | 0.9 | -1.311E-4 | -1.317E-4 | 0.5 | -1.210E-4 | -1.213E-4 | 0.2 |
| P1d | -1.377E-4 | -1.390E-4 | 0.9 | -1.310E-4 | -1.317E-4 | 0.5 | -1.210E-4 | -1.213E-4 | 0.2 |
| P1a≠P1d | 0.1% | 0.0% | | 0.1% | 0.0% | | 0.0% | 0.0% | |
| P2 | -7.896E-6 | -9.010E-6 | 12.4 | -8.744E-6 | -9.499E-6 | 7.9 | -8.803E-6 | -9.156E-6 | 3.9 |
| PT1 | 2.260E-7 | 2.818E-7 | 19.8 | 3.400E-7 | 3.628E-7 | 6.3 | 3.667E-7 | 3.644E-7 | 0.6 |
| PT2 | 2.535E-7 | 2.512E-7 | 0.9 | 3.309E-7 | 3.287E-7 | 0.7 | 3.531E-7 | 3.535E-7 | 0.1 |
| PT3 | 3.100E-7 | 3.521E-7 | 12.0 | 3.591E-7 | 3.648E-7 | 1.6 | 3.618E-7 | 3.599E-7 | 0.5 |
| ≠PT123 | 27.1% | 28.7% | | 7.9% | 9.9% | | 3.7% | 3.0% | |
| Var. Helic. | 4.419E-7 | | | 4.957E-7 | | | 1.201E-7 | | |
| Equation Unbalance | 1.500E-4<br>8.5 / 6.0 | -9.639E-5<br>4.6 / 3.4 | | 2.402E-5<br>1.2 / 0.9 | -1.540E-4<br>6.9 / 5.1 | | -1.977E-5<br>1.0 / 0.7 | -1.059E-4<br>4.8 / 3.6 | |

Table 8. Statistics of enstrophy transport equation for node 4 with varying refinements

| | Mesh 120 x 24 x 24 | | | Mesh 160 x 32 x 32 | | | Mesh 240 x 48 x 48 | | |
|---|---|---|---|---|---|---|---|---|---|
| | $2^{nd}$ order | $4^{th}$ order | ≠% | $2^{nd}$ order | $4^{th}$ order | ≠% | $2^{nd}$ order | $4^{th}$ order | ≠% |
| Aa | -2.009E-2 | -2.251E-2 | 10.8 | -2.206E-2 | -2.361E-2 | 6.6 | -2.269E-2 | -2.342E-2 | 3.1 |
| Ad | -2.009E-2 | -2.251E-2 | 10.8 | -2.206E-2 | -2.361E-2 | 6.6 | -2.269E-2 | -2.342E-2 | 3.1 |
| Aa≠Ad | 0.0% | 0.0% | | 0.0% | 0.0% | | 0.0% | 0.0% | |
| Ta | -2.386E-5 | -3.156E-5 | 24.4 | -3.504E-5 | -4.155E-5 | 15.7 | -4.128E-5 | -4.490E-5 | 8.1 |
| Td | -2.037E-5 | -2.960E-5 | 31.2 | -3.125E-5 | -3.957E-5 | 21.0 | -3.905E-5 | -4.397E-5 | 11.2 |
| Ta≠Td | 14.6% | 6.2% | | 10.8% | 4.8% | | 5.4% | 2.1% | |
| Df | -1.572E-3 | -2.094E-3 | 24.9 | -1.830E-3 | -2.190E-3 | 16.4 | -1.842E-3 | -2.006E-3 | 8.2 |
| Ds | 1.926E-2 | 2.788E-2 | 30.9 | 2.364E-2 | 2.986E-2 | 18.4 | 2.584E-2 | 2.889E-2 | 10.6 |
| Vu | -2.386E-2 | -3.100E-2 | 23.0 | -2.757E-2 | -3.242E-2 | 15.0 | -2.869E-2 | -3.097E-2 | 7.4 |
| Vu≠Df-Ds | 12.7% | 3.3% | | 7.6% | 1.1% | | 3.5% | 0.2% | |
| Un | -1.850E-2 | -2.041E-2 | 9.4 | -2.022E-2 | -2.142E-2 | 5.6 | -2.084E-2 | -2.140E-2 | 2.6 |
| Un≠Ad-Df | 0.1% | 0.0% | | 0.0% | 0.0% | | 0.0% | 0.1% | |
| P1 | 1.223E-4 | 1.611E-4 | 24.1 | 1.443E-4 | 1.712E-4 | 15.7 | 1.498E-4 | 1.624E-4 | 7.8 |
| P2 | 4.011E-3 | 4.494E-3 | 10.7 | 4.577E-3 | 4.906E-3 | 6.7 | 4.771E-3 | 4.929E-3 | 3.2 |
| P3 | 5.772E-3 | 5.765E-4 | 0.1 | 5.666E-3 | 5.642E-4 | 0.4 | 5.262E-4 | 5.244E-4 | 0.3 |
| PT | 1.083E-6 | 2.575E-6 | 57.9 | 2.138E-6 | 3.905E-6 | 45.2 | 3.706E-6 | 4.966E-6 | 25.4 |
| Var. Enstr. | -1.701E-4 | | | -1.220E-4 | | | -2.167E-5 | | |
| Equation Unbalance | -3.745E-3<br>18.6 / 13.3 | 2.522E-3<br>9.0 / 7.0 | | -1.623E-3<br>6.9 / 5.0 | 3.090E-3<br>10.3 / 8.0 | | -1.966E-4<br>0.8 / 0.6 | 2.143E-3<br>7.4 / 5.7 | |

An overall appreciation of the evolution of the transport equations unbalance is provided by table 9, showing the mean unbalances of the 18 nodes recorded, relative to the square root of the sum of the squared terms for the thre meshes used. Forth order show smaller mean errors, despite the nodes used in example. With varying rate, all unbalances diminish with refinement.

Table 9 – Mean per-cent unbalances among 18 nodes for varying mesh refinement

| Transport equation | 2nd order | | | 4th order | | |
|---|---|---|---|---|---|---|
| | Mesh 24 | Mesh 32 | Mesh 48 | Mesh 24 | Mesh 32 | Mesh 48 |
| Kin. En. (1st) | 16.8 | 11.1 | 7.1 | 9.8 | 8.4 | 6.1 |
| Kin. En. (2nd) | 23.2 | 13.4 | 7.8 | 18.8 | 12.4 | 6.0 |
| Helicity | 15.3 | 12.7 | 12.2 | 12,6 | 12.2 | 12.0 |
| Enstrophy | 20.6 | 12.1 | 5.2 | 13.8 | 7.2 | 3.7 |

**5.2. Velocity-vorticity statistical dynamic equation**

Finally, attention is turned to the statistical dynamic equation for the velocity-vorticity tensor, Eq. (26). Table 10 presents the fluctuating scalar properties kinetic energy, helicity and enstrophy, and the velocity-vorticity tensor for the selected nodes with mesh 240x48x48, comparing the values obtained by direct measurement of the tensor with those obtained via the statistical dynamic equation. Calculations were performed for time increment 0.0125, which was used in previous calculations, and a time increment four times smaller, 0.003125. The discrepancies between statistical dynamic estimates and direct measurements are enormous; results of the statistical dynamic equations are often one order of magnitude smaller than the value directly measured. The reduction in the time step affected statistical dynamic equations estimates as much as the values directly measured for the tensor and for the scalar properties: both show about 10% decrease with the smaller time increment.

Unless better approximations can be found by further research, this rough order of magnitude is the unique information that can be obtained. This is not useless information, for indicating the most relevant terms to be considered by means of other estimation method. This is illustrated in Table 11, showing the decomposition of the velocity-vorticity tensor for node 4 by the statistical dynamic method.

The most numerically relevant term is $\frac{1}{Re}\overline{u_\iota \int_o^t \frac{\partial^2 w_k}{\partial x_j \partial x_j} dt}$, which achieves order $10^{-4}$. Then follow terms $S_{kj}\overline{u_\iota \int_o^t w_j\, dt}$ , $W_j\overline{u_\iota \int_o^t s_{kj} dt}$ and $\overline{u_\iota \int_0^t \left[\partial(w_k u_j - w_j u_k)/\partial x_j\right] dt}$, which achieve order $10^{-5}$. Checks of precision are

Table 10 – Fluctuating scalar properties and velocity-vorticity tensor using different time steps for some nodes

| Node | Time increment | Energy Helicity Enstrophy | Velocity – vorticity tensor | | | | | |
|---|---|---|---|---|---|---|---|---|
| | | | Measured directly | | | Statistical dynamic equation | | |
| 4 | 1.25E-2 | 5.201E-5 | -5.4E-4 | -3.4E-4 | 6.3E-5 | -6.0E-5 | -5.9E-5 | 2.7E-4 |
| | | -1.588E-3 | -3.7E-4 | -2.5E-4 | -4.5E-4 | -6.0E-5 | -6.7E-5 | 1.7E-4 |
| | | 1.731E-2 | 1.0E-4 | 3.0E-5 | -7.9E-4 | -1.8E-5 | -3.1E-5 | -7.3E-5 |
| | 3.125E-3 | 4.690E-5 | -4.8E-4 | -3.1E-4 | 5.2E-5 | -5.4E-5 | -5.2E-5 | 2.4E-4 |
| | | -1.426E-3 | -3.3E-4 | -2.3E-4 | -4.1E-4 | -5.4E-5 | -6.0E-5 | 1.6E-4 |
| | | 1.552E-2 | 9.1E-5 | 2.7E-5 | -7.1E-4 | -1.7E-5 | -2.8E-5 | -6.2E-5 |
| 5 | 1.25E-2 | 6.355E-5 | 1.3E-12 | 9.1E-13 | 1.8E-4 | -6.2E-14 | 3.1E-13 | -1.8E-5 |
| | | 6.780E-12 | 1.2E-12 | 1.3E-12 | -7.0E-4 | -2.6E-13 | 2.2E-13 | 4.1E-4 |
| | | 2.002E-2 | 7.1E-22 | -1.6E-21 | 4.2E-12 | 9.4E-22 | 4.7E-22 | 3.0E-13 |
| | 3.125E-3 | 5.747E-5 | 1.1E-12 | 7.7E-13 | 1.6E-4 | -4.4E-14 | 2.6E-13 | 4.2E-4 |
| | | 5.797E-12 | 9.9E-13 | 1.1E-12 | -6.3E-4 | -2.1E-13 | 1.8E-13 | 3.7E-4 |
| | | 1.797E-2 | 6.2E-22 | -1.3E-21 | 3.6E-12 | 7.6E-22 | 3.9E-22 | 2.3E-13 |
| 9 | 1.25E-2 | 1.808E-5 | 7.9E-5 | 2.7E-5 | -6.1E-5 | -2.6E-5 | -2.1E-6 | -3.0E-6 |
| | | 3.260E-4 | 7.4E-5 | 1.6E-4 | 3.6E-5 | 4.0E-6 | -1.3E-5 | -2.3E-5 |
| | | 2.126E-3 | -6.6E-4 | 3.0E-5 | 8.6E-5 | 3.3E-5 | -2.6E-6 | -5.4E-6 |
| | 3.125E-3 | 1.674E-5 | 7.3E-5 | 2.5E-5 | -5.7E-5 | -2.4E-5 | -2.2E-6 | -3.0E-6 |
| | | 3.023E-4 | 6.9E-5 | 1.5E-4 | 3.3E-5 | 4.7E-6 | -1.2E-5 | -2.1E-5 |
| | | 1.962E-3 | -6.0E-5 | 2.8E-5 | 8.0E-5 | 3.0E-5 | -2.1E-6 | -4.6E-6 |

Table 11 Terms of velocity-vorticity statistical dynamic equation for node 4

| $\frac{\partial W_k}{\partial x_j}\overline{u_\iota \int_0^t u_j\, dt}$ | | | $\overline{S_{kj}u_\iota \int_o^t w_j\, dt}$ | | | $\overline{W_j u_\iota \int_o^t s_{kJ} dt}$ | | |
|---|---|---|---|---|---|---|---|---|
| -4.3E-6 | 3.1E-7 | -4.7E-6 | 8.7E-6 | 2.4E-5 | -3.8E-7 | 5.7E-6 | -4.2E-5 | 7.7E-6 |
| 4.7E-7 | 4.6E-8 | -4.8E-7 | 3.5E-5 | 6.43E-5 | -1.2E-7 | 3.8E-5 | -6.3E-5 | 5.8E-6 |
| 6.3E-6 | 3.2E-7 | 5.2E-6 | 4.4E-5 | 7.0E-5 | 3.0E-7 | 5.2E-5 | -4.5E-5 | -6.7E-7 |
| $u_i \int_0^t \frac{\partial (w_k u_j - w_j u_k)}{\partial x_j} dt$ | | | $\frac{1}{Re}\overline{u_\iota \int_o^t \frac{\partial^2 w_k}{\partial x_j \partial x_j} dt}$ | | | $\overline{u_\iota \int_0^t dt\, \frac{\partial (w_k u_j - w_j u_k)}{\partial x_j}}$ | | |
| -2.6E-6 | 2.9E-7 | -2.7E-7 | -8.0E-5 | -4.1E-5 | 2.6E-6 | -1.5E-6 | 2.2E-7 | -1.3E-7 |
| -9.8E-6 | 1.2E-6 | -5.2E-7 | -1.4E-4 | -6.8E-5 | 1.7E-4 | -5.0E-6 | 7.4E-7 | -4.5E-7 |
| 1.2E-5 | 1.6E-6 | -4.1E-7 | 1.1E-4 | -5.5E-5 | -6.8E-5 | -6.0E-6 | 8.9E-7 | -5.4E-7 |

included. The correlation $\overline{u_\iota \int_0^t u_j\, dt}$ of the first tensor is proved to be nil for $i = j$ (Figueiredo, 2016, 2018b); indeed the whole tensor values are small compared to the other terms. The correlation $\overline{u_\iota \int_0^t dt}$ that appears in the last tensor, which is neglected in the statistical dynamic equation since it is also nil for sufficiently high time interval, was introduced to check its possible influence; indeed its values are small.

## 6. CONCLUSION

The evaluation of the terms of the transport equations for kinetic energy, helicity and enstrophy have been demonstrated to converge with space and time refinements. The present estimates of the statistical dynamic equation, provided very poor quantitative representation of the velocity-vorticity tensor, which may be useful for indicating the most important terms, but can not be seen as a method of calibration. Better estimates are expected by further matching the Runge-Kutta integration of the Navier-Stokes solver and the Simpson integration of the statistics processing.

In the present Cartesian semi-staggered mesh, increasing the order of velocity and vorticity derivatives was simple, but increasing the order of pressure derivatives was more complex due to the staggered position of pressure with respect to the velocities. No such difficulty would exist for collocated meshes. In fully staggered mesh, conversion of all velocity data to the pressure nodes employs only one-dimensional interpolations; in principle, a third order polynomial interpolation analogous to Eq. (36) can be used, providing forth order approximation of all velocity components at the pressure location. Upon such collocated field, forth order interpolations of Eqs. (33) to (35) can be employed.

The program for evaluation of the terms of the transport equations of the scalars is ready for the subsequent work, translation to a language suitable for multiprocessing, such as Python for application to effectively turbulent phenomena via DNS or LES computations. Interest on engaging in this research was manifested by professors Aristeu Silveira Neto, from UFU and Rogério Gonçalves dos Santos, from UNICAMP (private communications); both have access to computational clusters and experience with parallel computation. Professor Silveira Neto employs program MFSim, developed collectively at UFU, which is suitable for RANS, URANS and LES computations, using Cartesian staggered meshes and fractional step coupling of pressure and continuity. Professor Santos is engaged in the developments of two programs for multiprocessors computation: the referred Finite Volume NavSto program for incompressible flow, and a high order Finite Difference program for compressible flows, which treats the incompressible flow as a limiting case.

Participation of other researchers is welcome as extremely important for mutual checking and for enlarging the range of situations analyzed, all community is invited to participate in the adventure of creating the kinetic energy – helicity turbulence model.

## 7. REFERENCES

Allen, D.N.G., Sauthwell, R.V., 1955. "Relaxation Methods Applied to Determine the Motion, in Two Dimensions, of a Viscous Flow Pasta Fixed Cylinder". *Quarterly J. Mechanics and Applied Mathematics*, v.8, 129-145.

Davidson, P.A., 2004. *Turbulence - An Introduction for Scientists and Engineers*, Oxford University Press, Oxford

Llagostera, J. e Figueiredo, J. R., 2000a. "Numerical study on mixed convection in a horizontal flow past a square cavity using UNIFAES scheme" *J. Braz. Society Mech. Sciences*, v.22, 4, 583-597.

Llagostera, J. e Figueiredo, J. R., 2000b. "Application of the UNIFAES discretization scheme to mixed convection in a porous layer with a cavity, using the Darcy model". *J. Porous Media*, v.3, 2, 16

Figueiredo, J. R., 1997. "A unified finite-volume finite-differencing exponential-type scheme for the convective-diffusive fluid transport equations". *Journal of the Brazilian Society of Mechanical Engineers*, v.19, n.3, 371-391

Figueiredo, J. R. e Llagostera, J., 1999. "Comparative study of the unified finite approach exponential-type scheme

(UNIFAES) and its application to natural convection in a porous cavity", *Numerical Heat Transfer, B*, v.35, 3, 347-367

Figueiredo, J. R. e Oliveira, K. P. M., 2009a. "Comparative study of UNIFAES and other finite-volume schemes for the discretization of advective and viscous fluxes in incompressible Navier-Stokes equations, using various mesh structures". *Numerical Heat Transfer, B*, v.55, 5, 406-434

Figueiredo, J. R. e Oliveira, K. P. M., 2009b. "Comparative study of the accuracy of the fundamental mesh structures for the numerical solution of incompressible Navier-Stokes equations in the two-dimensional cavity problem". *Numerical Heat Transfer, B*, v.55, 5, 406-434

Figueiredo, J.R. 2016 "A dynamic statistical equation based model for the turbulent transport of kinetic energy in shear layes". *Proceedings of Spring School in Transition and Turbulence, EPTT 2016* S. José dos Campos, SP, Brazil.

Figueiredo, J.R. 2018a "Towards a kinetic energy – helicity turbulence model". *Proceedings of Spring School in Transition and Turbulence EPTT 2018*, Uberlandia, MG, Brasil.

Figueiredo, J.R. 2018b "A statistical dynamic model for the turbulent transport of kinetic energy in shear layers". *J. Aerosp. Technol. Manag.* 10:e2518, doi:10.5028/jatm.v10.915

Karki, K., Mongia, H., Patankar, S.V., 1989. "Solution of three-dimensional flow problems using a flux-spline method." 27th Aerospace Science Meeting, AIAA.

Nascimento, A.H.G., 2019. *Numerical Solution of Incompressible Flows in Plane Channels with Gradual Expansions (in Portuguese)* M.Sc. Thesis, Unicamp, Campinas.

Nascimento, A.H.G., Rodrigues, G.S., Figueiredo, J.R. 2020. *A semi-staggered finite volume approach applied to two- and three- dimensional flow in channels with gradual expansions.* Submitted to the Journal of Computational Physics.

Patankar, S.V., 1980. *Numerical Heat Transfer and Fluid Flow*, Mc-Graw Hill Inc.

Pope, S.B., 2000, *Turbulent Flows*, Cambridge University Press, Cambridge, pp.325-327

Prakash, C. 1984. "Application of the locally analytic differencing scheme to some test problems" *Numerical Heat Transfer*, v.7, n.2, 165-182

Rathby, G., Torrance, K. 1974, "Upstream-weighted differencing schemes and their application to elliptic problems involving fluid flow." *Computers and Fluids*, v.2, n.2, 191-206

Rhie, C.M., Chow, W.L., 1983. "Numerical study of the Turbulent flow past an airfoil with trailing edge separation." *AIAA Jounal*, v.21, n.11, 1525-1532

Rodrigues, G.S., 2019. *Performance of Finite Volume Discretization Schemes in Advective-Diffusive Transport Equation (in Portuguese)* M.Sc. Thesis, Unicamp, Campinas.

Rodrigues, G.S., Nascimento, A. H., Figueiredo, J. R., 2020. Assessment of seven *finite volume schemes for linear and nonlinear advective-diffusive equation. Submitted to International Journal for Numerical Methods in Fluids*

Santos, R. G.; Figueiredo, J. R., 2011. "Numerical simulation study in a three-dimensional backward-facing step flow", 21st International Congress of Mechanical Engineering, Buenos Aires, Argentina.

Spalding, D.B., 1972. "A novel finite difference formulation for differential expressions involving both first and second derivatives." *International Journal for Numerical Methods in Engineering*, v.4, n.4, 551-559.

Varejão, L.M.C., 1979. *Flux-Spline Method for Heat and Momentum Transfer*, Ph. D Thesis, University of Minnesota, Mineapolis

Wong, H.H.; Raithby, G.D., 1979, "Improved finite-difference methods based on a critical evaluation of the approximation errors." *Numerical Heat Transfer*, v.2, n.2, 139-163

Tennekes, H. ; Lumley, J.L., 1972, *A First Course in Turbulence*, MIT Press, Cambridge, Massachusetts

## 7. RESPONSIBILITY NOTICE

The author is the only responsible for the printed material included in this paper.